Computers and Electronics in Agriculture 104 (2014) 32–39

Contents lists available at ScienceDirect

Computers and Electronics in Agriculture

journal homepage: www.elsevier.com/locate/compag

Analysis of wave velocity patterns in black cherry trees and its effect on internal decay detection

Guanghui Li [a,*], Xiping Wang [b], Hailin Feng [a], Jan Wiedenbeck [c], Robert J. Ross [b]

[a] School of Information Engineering, Zhejiang Agriculture and Forestry University, Hangzhou, China
[b] USDA Forest Service Forest Products Laboratory, Madison, WI, USA
[c] USDA Forest Service, Northern Research Station, Princeton, WV, USA

A R T I C L E   I N F O

Article history:
Received 10 December 2013
Received in revised form 3 March 2014
Accepted 21 March 2014

Keywords:
Stress wave
Velocity pattern
Trees
Internal decay detection
Tomography

A B S T R A C T

In this study, we examined stress wave velocity patterns in the cross sections of black cherry trees, developed analytical models of stress wave velocity in sound healthy trees, and then tested the effectiveness of the models as a tool for tree decay diagnosis. Acoustic tomography data of the tree cross sections were collected from 12 black cherry trees at a production forest. Trees were subsequently cut, and the disk at each test location was obtained to assess the true physical condition. Stress wave velocity data of different paths across grain, from radial to tangential, were extracted from the acoustic tomography data sets. Our analysis indicated that the ratio of tangential velocity to radial velocity in sound healthy trees approximated a second-order parabolic curve with respect to the symmetric axis $\theta = 0$ (θ is the angle between wave propagation path and radial direction). The analytical model was found in excellent agreement with the real data from healthy trees. Further examination indicated that the analytical model can be used to diagnose internal conditions of trees when a stress wave testing method is used in tree inspection.

1. Introduction

Forests are an extremely valuable resource to human beings. Internal decay of trees endangers the health of forests and decreases the quality and value of timber. Detection of tree decay is important not only to forest management but also to public safety in urban communities. The stress wave method has been well recognized as a robust and low-cost nondestructive technique to test living trees and wood structure for internal conditions. Stress wave transmission time increases dramatically in decayed areas, and internal defects can be detected by the time difference between measured value and the reference value (Pellerin and Ross, 2002). Several commercial stress wave testing tools are available to conduct single path stress wave measurements in wood. In addition, some sonic tomography equipment (e.g., ArboSonic 2D, PiCUS Sonic Tomograph, and Arbotom) have been developed to conduct multipath stress wave measurements on trees and construct two-dimensional or three-dimensional tomograms of tree cross sections. An accurate understanding of wave velocity patterns in trees is therefore important to the diagnosis of internal decay, and it is also critical to developing reliable and effective imaging software for internal decay analysis (Bucur, 2003).

To improve the precision of decay detection, many researchers studied the relationships between wood mechanical characteristics and stress wave velocity. Dikrallah et al. (2006) presented an experimental analysis of acoustic anisotropy of wood, in particular the dependence of propagation velocities of stress waves on natural anisotropy axis in the cross section. They found a significant difference in wave velocity between the waves propagating in whole volume and the waves guided on bars. Maurer et al. (2005) studied the anisotropy effects on time-of-flight based tomography, and they assumed elliptic anisotropy, where the angle dependent velocity v can be written as $v = v_{radial}\,(1 - \varepsilon\,\sin(\phi - \varphi)^2)$, where ϕ is the ray angle. φ represents the azimuth of the v_{radial} direction relative to the axis of the coordinate system, and ε specifies the degree of anisotropy.

Kazemi et al. (2009) found that the ultrasonic velocity changed in different heights of beech tree and different directions. It was seen that the ultrasonic velocity in tangential direction was minimum. Then it increased and reached a maximum in radial direction. Liang et al. (2010) showed that stress waves traveled fastest in radial direction and that velocity decreased as the wave propagation path shifted toward to tangential direction. Velocity

* Corresponding author. Tel.: +86 57163740788.
E-mail addresses: lgh@zafu.edu.cn (G. Li), xwang@fs.fed.us (X. Wang), sealinfeng@gmail.com (H. Feng), jwiedenbeck@fs.fed.us (J. Wiedenbeck), rjross@fs.fed.us (R.J. Ross).

http://dx.doi.org/10.1016/j.compag.2014.03.008
0168-1699/

also increased as the number of annual rings increased. Gao et al. (2012) investigated the effect of environment temperature on acoustic velocity of standing trees and green logs and developed workable models for compensating temperature differences as acoustic measurements were performed in different climates and seasons. Their results indicated that acoustic velocity increased as wood temperature decreased when the temperature was below the freezing point. When the temperature was well above freezing, velocity decreased linearly at a slow rate as wood temperature increased.

The objectives of this study were to investigate the stress wave velocity patterns in cross sections of standing trees and examine the effect of internal tree decay on the velocity pattern. We proposed a theoretical model of stress wave velocity in sound healthy trees and tested the effectiveness of the model as a tool for decay diagnosis.

2. Theoretical analysis of wave velocity pattern

With the assumption that the trunk of a tree under test is cylindrical body, and its cross section is in ideal circularity (Fig. 1), and the pith is located in the center of the circular tree, we now consider the relationship between stress wave velocity and its propagation direction. In Fig. 1, S is a source sensor, and R_0, R_1 and R_2 are receiver sensors. Stress wave is transmitted from the source to the receivers. SR_0 represents the radial direction R, and SR_1 and SR_2 represent the tangential direction T. The dynamic modulus of elasticity (E, Pa) can be calculated from the stress wave velocity (V, m/s) using the following equation:

$$E = V^2\rho \tag{1}$$

where ρ is the density of wood (kg/m^3).

Given the angle θ between radial and tangential directions, let E_R, E_T, and G_{RT} represent radial modulus of elasticity, tangential modulus of elasticity, and shear modulus, respectively. υ_{RT} represents Poisson's ratio of wood material, then we have

$$\overline{E}_R = \frac{1}{\overline{S}_R},\quad \overline{E}_T = \frac{1}{\overline{S}_T};\quad \overline{G}_{RT} = \frac{1}{\overline{S}_{RT}} \tag{2}$$

$$\overline{S_R} = \frac{\cos^4\theta}{E_R} + \frac{\sin^4\theta}{E_T} + \left(\frac{1}{G_{RT}} - \frac{2\upsilon_{RT}}{E_R}\right)\sin^2\theta\cos^2\theta \tag{3}$$

$$\overline{S_T} = \frac{\cos^4\theta}{E_T} + \frac{\sin^4\theta}{E_R} + \left(\frac{1}{G_{RT}} - \frac{2\upsilon_{RT}}{E_R}\right)\sin^2\theta\cos^2\theta \tag{4}$$

$$\overline{S_{RT}} = 4\left(\frac{1}{E_R} + \frac{1}{E_T} + \frac{2\upsilon_{RT}}{E_R}\right)\sin^2\theta\cos^2\theta + \frac{1}{G_{RT}}(\sin^2\theta - \cos^2\theta)^2 \tag{5}$$

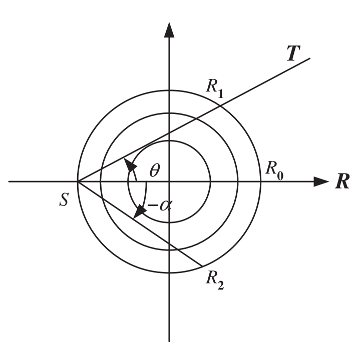

Fig. 1. The coordinate system of cross-section plane.

From Eqs. (1)–(5), the relationship between the stress wave velocity V and angle θ can be given as follows (Dikrallah et al., 2006).

$$V_T = V_R\cos^2\theta\sqrt{1 + \frac{E_T}{E_R}\tan^4\theta + 2\frac{G_{RT}}{E_R}\tan^2\theta} \tag{6}$$

where V_T is the tangential velocity and V_R is the radial velocity. Now we can approximate Eq. (6) with second order Taylor polynomial. Let $f(\theta)$ represent the ratio of V_T to V_R, then

$$f(\theta) = \cos^2\theta\sqrt{g(\theta)} \tag{7}$$

where

$$g(\theta) = 1 + \frac{E_T}{E_R}\tan^4\theta + 2\frac{G_{RT}}{E_R}\tan^2\theta. \tag{8}$$

From Eqs. (7) and (8), the derivatives of $f(\theta)$ and $g(\theta)$ can be determined as

$$\begin{aligned} g'(\theta) &= 4\frac{E_T}{E_R}\tan^3\theta(\tan\theta)' + 4\frac{G_{RT}}{E_R}\tan\theta(\tan\theta)' \\ &= 4\frac{E_T}{E_R}\frac{\tan^3\theta}{\cos^2\theta} + 4\frac{G_{RT}}{E_R}\frac{\tan\theta}{\cos^2\theta} = \frac{4}{E_R}\frac{\tan\theta}{\cos^2\theta}(E_T\tan^2\theta + G_{RT}) \end{aligned} \tag{9}$$

$$\begin{aligned} g''(\theta) &= \frac{4}{E_R}\left(\left(\frac{\tan\theta}{\cos^2\theta}\right)'(E_T\tan^2\theta + G_{RT}) + \frac{\tan\theta}{\cos^2\theta}(E_T\tan^2\theta + G_{RT})'\right) \\ &= \frac{4}{E_R}\sec^2\theta((\sec^2\theta + 2\tan^2\theta)(E_T\tan^2\theta + G_{RT}) \\ &\quad + 2E_T\tan^2\theta\sec^2\theta) \end{aligned} \tag{10}$$

$$\begin{aligned} f'(\theta) &= (\cos^2\theta)'\sqrt{g(\theta)} + \cos^2\theta(\sqrt{g(\theta)})' \\ &= -\sin 2\theta\sqrt{g(\theta)} + \frac{1}{2}\cos^2\theta g^{-1/2}(\theta)g'(\theta) \end{aligned} \tag{11}$$

$$\begin{aligned} f''(\theta) &= -(\sin 2\theta)'\sqrt{g(\theta)} - \sin 2\theta(\sqrt{g(\theta)})' + \frac{1}{2}(\cos^2\theta)'g^{-1/2}(\theta)g'(\theta) \\ &\quad + \frac{1}{2}\cos^2\theta(g^{-1/2}(\theta)g'(\theta))' = -2\cos 2\theta\sqrt{g(\theta)} \\ &\quad - \frac{1}{2}\sin 2\theta g^{-1/2}(\theta)g'(\theta) - \frac{1}{2}\sin 2\theta g^{-1/2}(\theta)g'(\theta) \\ &\quad + \frac{1}{2}\cos^2\theta\left(-\frac{1}{2}g^{-3/2}(\theta)g'(\theta)g'(\theta) + g^{-1/2}(\theta)g''(\theta)\right) \end{aligned} \tag{12}$$

From Eqs. (7)–(12), we know

$$g(0) = 1,\quad g'(0) = 0,\quad g''(0) = 4\frac{G_{RT}}{E_R}$$

$$f(0) = 1,\quad f'(0) = 0,\quad f''(0) = -2\left(1 - \frac{G_{RT}}{E_R}\right) \tag{13}$$

So, function $f(\theta)$ can be expanded to Taylor series at $\theta = 0$ as follows:

$$\begin{aligned} f(\theta) &= f(0) + \frac{1}{1!}f'(0)\theta + \frac{1}{2!}f'(0)\theta^2 + O(\theta^3) \\ &= 1 - \left(1 - \frac{G_{RT}}{E_R}\right)\theta^2 + O(\theta^3), \end{aligned} \tag{14}$$

$$\approx 1 - \left(1 - \frac{G_{RT}}{E_R}\right)\theta^2 \tag{15}$$

where O (θ^3) is the remainder of the Taylor polynomial. For the coordinate system given in Fig. 1, we assume the angle $\theta > 0$ if θ is counter-clockwise from the radial direction. Otherwise, $\theta < 0$ if θ is clockwise from the radial direction. Eq. (14) shows that the ratio of V_T to V_R approximates a parabolic curve with the symmetric axis

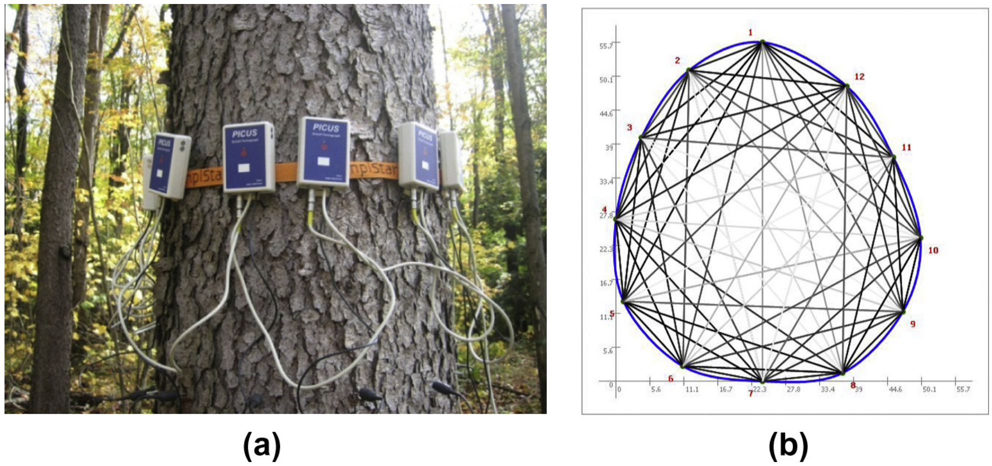

Fig. 2. Sonic tomography test on black cherry trees using a PiCUS Sonic Tomograph tool. (a) Sensor arrangement and (b) stress wave propagation paths.

$\theta = 0$. For a real living tree, its cross section may not be in ideal circularity. Therefore, the velocity pattern may deviate from the theoretical model shown by Eqs. (14) and (15).

3. Materials and methods

The experimental data used in this study were from an early investigation on tree decay detection (Wang et al., 2009). The field test site was located just south of Kane, Pennsylvania, in McKean County and was part of the Collins Pennsylvania Forest. Twelve black cherry trees were selected as test samples through visual examination and single-pass stress wave test. These selected trees had a wide range of physical conditions in terms of physiological characteristics and stress wave transmission times. For each sample tree, we conducted acoustic tomography tests at three different heights (i.e., 50 cm, 100 cm, and 150 cm) above the ground, and one unique label was used to mark the cross section. For example, "4–50" represents the sample tree No. 4 and the test height is 50 cm. Fig. 2 shows the acoustic tomography test on a black cherry tree sample using a PiCUS Sonic Tomograph tool (Argus Electronic GmbH, Rostock, Germany). The PiCUS Sonic Tomograph measurement system consisted of 12 sensors, which were evenly placed around the trunk in a horizontal plane (Fig. 2a). Stress wave transmission times were measured by sequentially tapping each pin of the sensors using a steel hammer. For each source sensor, the other 11 sensors receive the stress wave signals, and the wave transmission times were recorded by the system. A complete data matrix was obtained through this measurement process at each test location. Fig. 2b shows the sensor arrangement and the paths of stress wave measurements on one cross section.

4. Experimental results and analysis

4.1. Trees without decay

Among the selected samples were eight cross sections (Nos. 4–150, 7–50, 10–50, 11–50, 12–50, 15–50, 16–50, and 17–50) revealed as in sound condition after the trees were cut. As an example, Table 1 shows the velocity measurements of sample No. 17–50 with the sequential number 1–12 representing the source points, and the angle θ representing the position of the receiver points relative to the source point, as defined in Fig. 1. For simplicity, the average of the line velocities of the measurement paths with same angle θ from all the 12 source points was calculated. For solid cross section, the velocity in radial direction V_R (with $\theta = 0$) was the highest, and the velocity in tangential direction V_T (with $\theta = \pm 75^\circ$) was the lowest. Consider the tangential velocity at $\theta = \pm 75^\circ$ as a reference velocity, then the ratio of V_T to V_R reflects the wave velocity patterns in a tree cross section.

Fig. 3 shows the wave velocity pattern under source point 1. Here, the angle θ was converted into radian unit ($1^\circ = \pi/180$). The relationship between velocity ratio V_T/V_R and angle θ was statistically in a parabolic curve, with a coefficient of determination $R^2 = 0.985$. The coefficients of the second order polynomial regression are $a = -0.176$, $b = 0.00023$, and $c = 0.9951$. It was noted that the coefficient of the first order term was close to zero and the con-

Table 1
Acoustic velocity data for tree sample 17–50 (Unit: m/s).

θ (°)	Source point												Average	V_t/V_r
	1	2	3	4	5	6	7	8	9	10	11	12		
75	1023	888	1013	974	921	875	896	861	874	919	1014	930	932.33	0.636
60	1181	1204	1132	1208	1109	1098	1054	986	1143	1146	1209	1201	1139.25	0.777
45	1354	1280	1293	1339	1243	1161	1249	1161	1309	1332	1394	1311	1285.5	0.877
30	1408	1426	1382	1430	1266	1339	1374	1293	1329	1465	1473	1443	1385.67	0.945
15	1503	1482	1400	1446	1409	1412	1449	1424	1392	1486	1535	1459	1449.75	0.989
0	1500	1447	1360	1541	1434	1456	1462	1469	1397	1505	1528	1500	1466.58	1
−15	1441	1427	1419	1556	1447	1354	1482	1478	1374	1481	1538	1469	1455.5	0.999
−30	1400	1459	1378	1538	1372	1308	1435	1410	1299	1442	1476	1368	1407.08	0.9599
−45	1353	1364	1304	1359	1278	1234	1294	1312	1231	1333	1310	1269	1303.42	0.889
−60	1211	1261	1089	1233	1182	1054	1167	1208	1100	1120	1191	1169	1165.42	0.795
−75	1035	1066	836	1139	927	843	976	993	986	911	1046	909	972.25	0.663

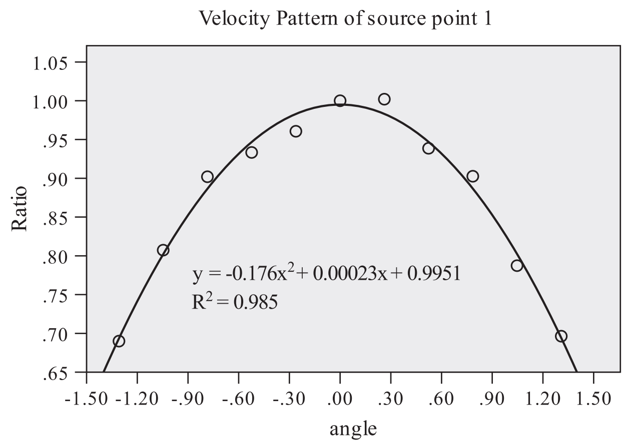

Fig. 3. Wave velocity pattern under source point 1 for sample 17–50.

stant close to 1, which is in good agreement with Eqs. (14) and (15). Actually, all the wave velocity patterns under different source points were parabolic curves as shown in Fig. 4a. The tomogram of the cross section No. 17–50 taken by the PiCUS Sonic Tomograph system is shown in Fig. 4b, which indicates the cross section in a sound condition.

Ideally, if a tree trunk is considered as transversely isotropic material, the velocity values obtained from the same measurement paths (e.g., 75° and −75° from radial direction) should be the same or very close. The average velocity for the same measurement paths under different source points was tabulated in Table 1.

Fig. 5 shows the average wave velocity pattern for the cross section No. 17–50. The trend line of ratio V_t/V_r is still a second order parabolic curve ($y = ax^2 + bx + c$) with the coefficients $a = -0.2062$, $b = -0.0096$, $c = 1.0067$, and the coefficient of determination $R^2 = 0.9989$. This result is in a good agreement with Eq. (15).

The experimental results indicated that all other sound samples (cross sections) had the similar velocity patterns as sample No. 17–50. The regression relationships between velocity ratio (V_T/V_R) and wave propagation path angle θ are shown in Table 2.

From Table 2, it can be seen that for the sound black cherry trees there exists a second order polynomial relationship ($y = ax^2 + bx + c$) between the velocity ratio V_T/V_R and wave propagation path angle θ. A close examination of the correlation coefficients indicated that this relationship can be expressed as the following general form:

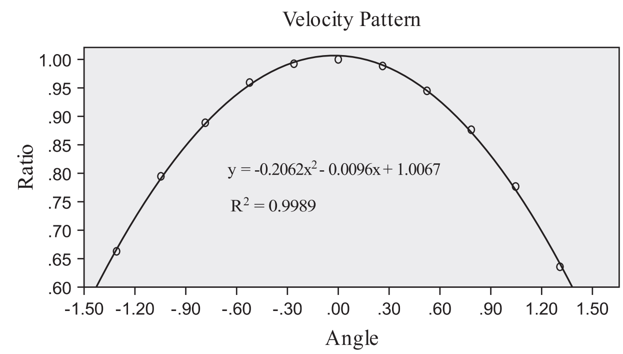

Fig. 5. The average wave velocity pattern of sample 17–50.

Table 2
Equations for parabolic curves fit to velocity ratio (V_t/V_r) and propagation path (θ) data.

Sample no.	a	b	c	R^2
4–150	−0.1957	0.0137	1.0049	0.994
7–50	−0.1992	0.0009	1.0209	0.9919
10–50	−0.2114	0.005	1.0243	0.9885
11–50	−0.2275	0.0026	1.0113	0.9973
12–50	−0.2182	−0.0041	1.0132	0.996
15–50	−0.1855	−0.0103	1.0507	0.9542
16–50	−0.1842	−0.0028	0.9852	0.9916
17–50	−0.2062	−0.0096	1.0067	0.9989
Average	−0.2031	−0.0006	1.0147	0.9891

$$y = 1 + ax^2 \tag{16}$$

where the coefficient $a \approx -0.2$, $y = V_T/V_R$, $x = \theta$. According to Eq. (15) we proposed earlier, $a = -(1 - G_{RT}/E_R)$ should be determined by the mechanical properties of the tree trunk. The stress wave data obtained from the black cherry tree samples showed that Eq. (15) is valid for describing the wave velocity patterns in the cross section of a tree trunk.

4.2. Trees with internal decay

The tomography results from the black cherry tree samples showed that twelve cross sections had internal defects. These samples were 1–50, 1–100, 1–150, 2–50, 4–50, 4–100, 18–50, 18–100, 18–150, 19–50, 19–100, 19–150. Fig. 6 shows the pictures of the

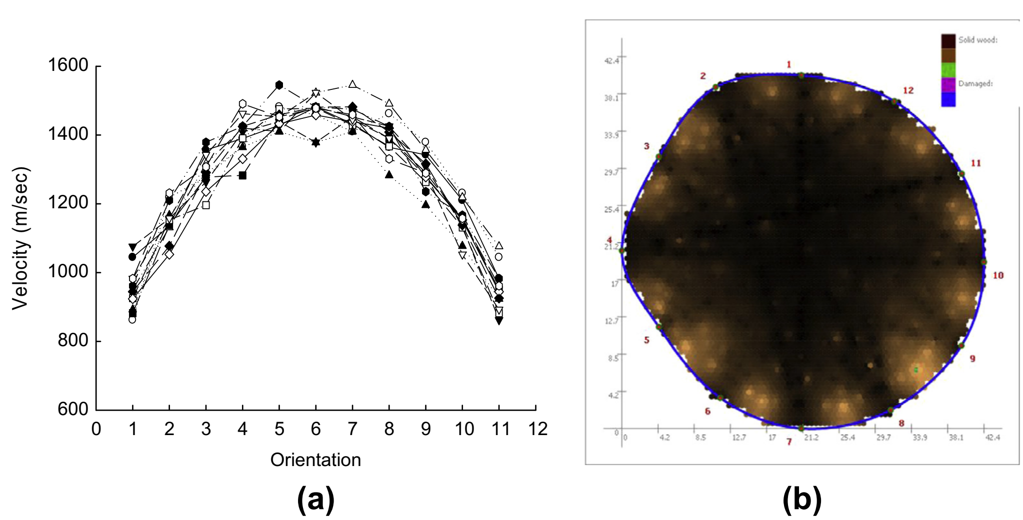

Fig. 4. The velocity trend lines and tomogram of sample 17–50. (a) Measured acoustic velocity patterns. (b) Acoustic tomogram.

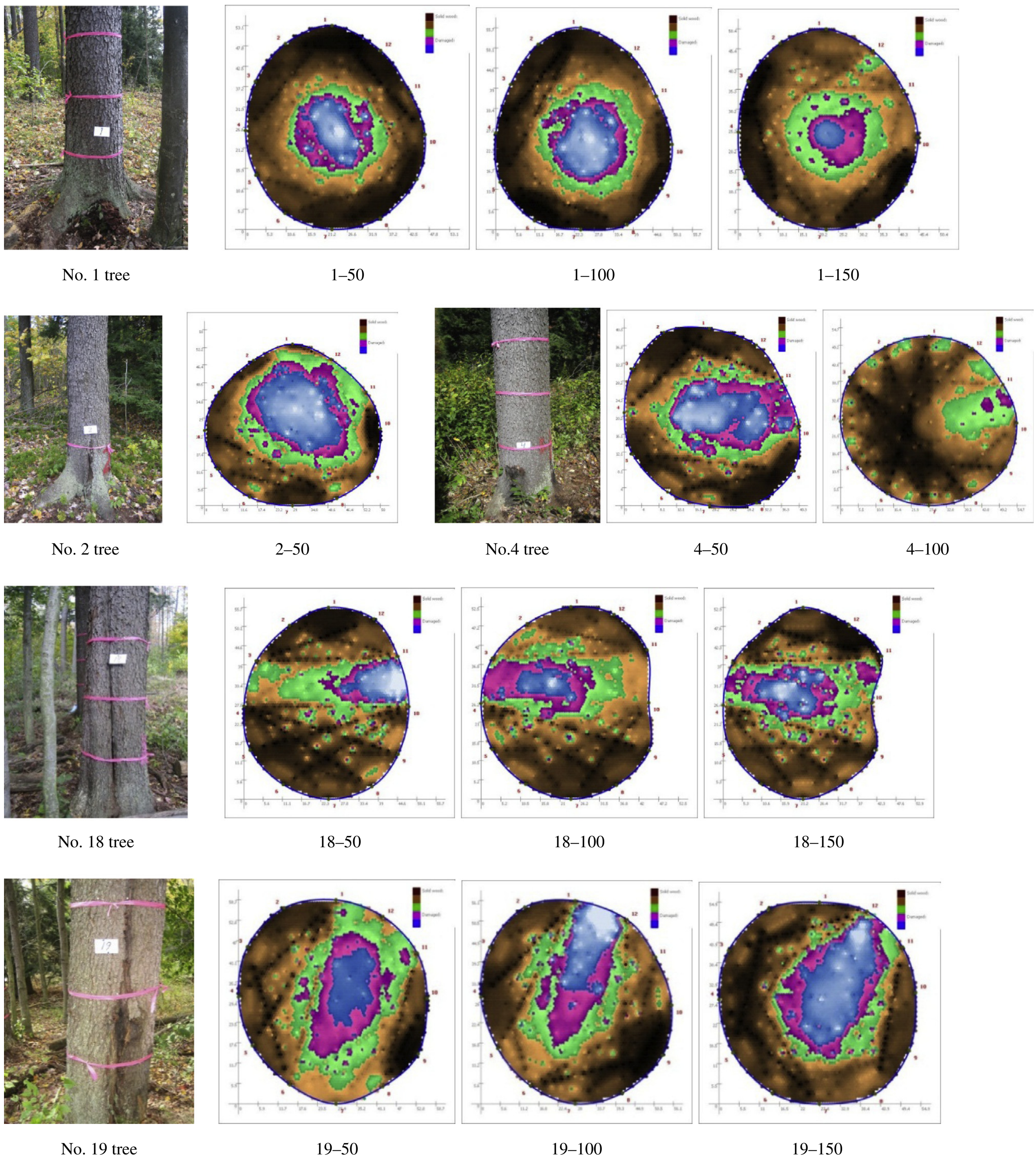

Fig. 6. Black cherry trees and their tomograms showing internal defects.

tree samples with internal defects and the corresponding tomograms. Fig. 7 displays the corresponding velocity pattern of each tree cross section where the acoustic tomography test was performed.

The structural defects found in tree #1 were the most significant of all tested trees with both tomograms and disk samples confirming heartwood decay at all three heights. Laboratory examination confirmed the presence of brown-rot decay fungus. The tomograms of tree #1 at 50-, 100-, and 150-cm heights showed large acoustic shadows in the central areas of the cross sections. The size of the shadow was the largest at the lower height (50 cm) and decreased progressively as the test height increased. The velocity patterns for tree #1 in Fig. 7 show a very different shape compared with that found in sound trees. The stress wave velocity was the lowest in the radial paths at all three heights, as opposed to be the highest in sound trees. This "caved shape" in measured velocity pattern corresponded to the "acoustic shadow" found in the tomogram very well.

In addition, both tomograms and wave velocity pattern figure show that cross sections 2–50 and 4–50 have the same cases as

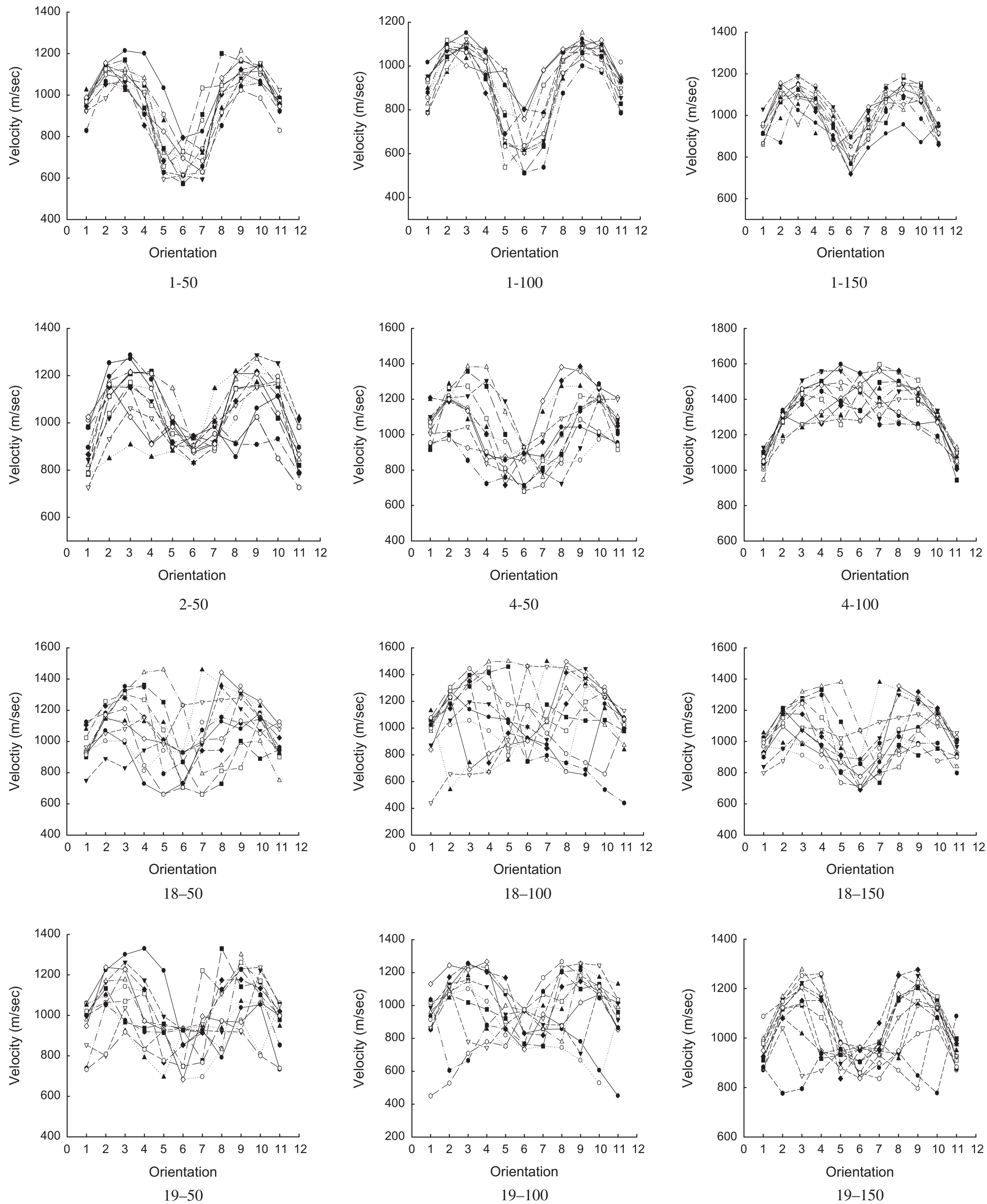

Fig. 7. Velocity patterns of the black cherry trees with internal defects.

tree #1, but 4–100 has only a light internal defect. Tree #19 has a clear crack from its outside, and the tomograms of three cross sections 19–50, 19–100, and 19–150 demonstrate the crack and central decay, so the velocities decrease in the sixth direction dramatically for all the source points. Tree #18 also had internal decay and a crack, but the decay area does not surround the central point, which resulted in a velocity pattern that is more complex than tree #19 as shown in cross sections 18–50 and 18–100.

5. Discussion

An acoustic tomography tool typically applies 8–12 or even more sensors to acquire wave velocity data, and then generates a two-dimensional tomogram for each cross section tested. The measurement process is time consuming because of the delicate procedures for setting up sensors and conducting a series of time-of-flight tests. For practical use in field, it is often desirable to use far fewer sensors and complete tests in a short period of time but still obtain reasonably accurate and sufficient data enabling the detection of internal tree decay.

Based on our theoretical analysis and experimental results, we propose to use the established velocity patterns in healthy trees as a standard model to diagnose the internal tree decay. A reference velocity V_0 can be determined by calculating the average of the line velocities of the neighboring sensors, the wave propagation path angle θ of V_0 is 75° for the case of 12 sensors. This velocity can be used as a reference because typically the sapwood of a tree is intact (Divos and Divos, 2005). According to Eqs. (14) and (15),

$$V_0/V_r \approx 1-\left(1-\frac{G_{RT}}{E_R}\right)\left(\frac{75\pi}{180}\right)^2 = 1-\left(1-\frac{G_{RT}}{E_R}\right)\left(\frac{5\pi}{12}\right)^2 \tag{17}$$

Now, the velocity $V(\theta)$ can be determined by the following equation:

$$V(\theta)/V_0 \approx \left(1-\left(1-\frac{G_{RT}}{E_R}\right)\theta^2\right)\bigg/\left(1-\left(1-\frac{G_{RT}}{E_R}\right)\left(\frac{5\pi}{12}\right)^2\right) \tag{18}$$

Therefore the trend line of velocity ratio $V(\theta)/V_0$ is also a parabolic curve with the symmetric axis $\theta = 0$. Fig. 8 shows the trend line of ratio $V(\theta)/V_0$ for cross section 17–50.

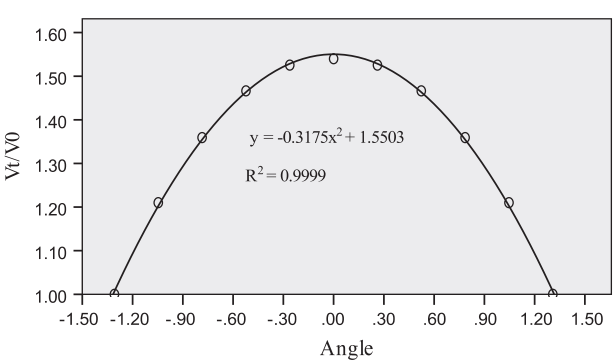

Fig. 8. The trend line of ratio $V(\theta)/V_0$ of 17–50.

When the reference velocity V_0 is determined, the other line velocities can be estimated by Eq. (18) and an inference of whether this line is a defect line or not can be made accordingly. Based on the theoretical velocity model and the measured velocity patterns, we can also evaluate the internal decay in a tree trunk without determining a reference velocity V_0. From the theoretical analysis, the velocity pattern of a sound tree trunk exhibits a second-order parabolic curve similar to the velocity ratio V_T/V_R. As an example,

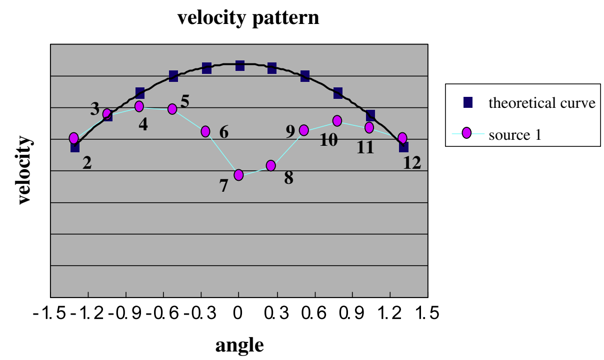

Fig. 9. Theoretical velocity pattern and measured velocity data.

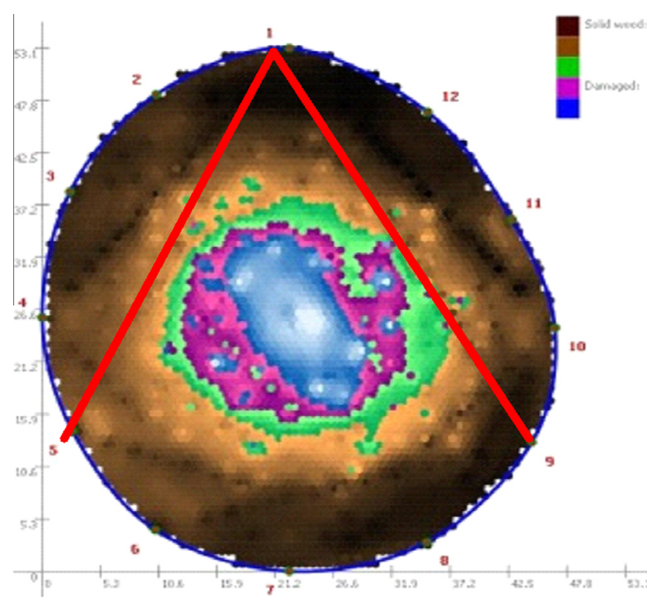

Fig. 10. Tomogram of sample 1–50.

Table 3
Acoustic velocity data of sample 1–50 (unit: m/s).

Test point	1	2	3	4	5	6	7	8	9	10	11	12
1		917	1150	1228	1217	1024	825	823	1040	1106	1069	940
2	999		965	1170	1228	1090	947	730	905	1055	1083	1113
3	1150	881		1025	1190	1111	1035	654	599	651	915	1067
4	1199	1053	923		997	1086	1127	1067	729	616	609	1014
5	1184	1100	1096	972		933	1143	1151	867	766	573	801
6	1044	1003	1103	1145	1019		960	1107	1047	999	679	657
7	764	521	972	1119	1143	953		936	1024	1046	849	677
8	826	661	606	1097	1189	1143	955		936	1125	1028	860
9	1048	849	624	712	1008	1105	1080	1040		1033	1063	999
10	1110	949	539	613	720	1026	1086	1185	1018		969	994
11	1064	991	901	646	574	635	858	1057	1055	877		798
12	996	1083	1094	1100	1012	798	689	973	1048	977	861	

Table 3 shows the measured velocity data for sample 1–50. Fig. 9 illustrates the theoretical velocity model of the black cherry and the measured velocity data under source point 1, and Fig. 10 shows the tomogram of sample 1–50.

It can be seen from Table 3 that, from source point 1, the wave velocities were 999 m/s (1–2), 1150 m/s (1–3), 1199 m/s (1–4), 1184 m/s (1–5), 1044 m/s (1–6), 764 m/s (1–7), 826 m/s (1–8), 1048 m/s (1–9), 1110 m/s (1–10), 1064 m/s (1–11), and 996 m/s (1–12). From Fig. 9, it can be seen that the line velocities of 1–5, 1–6, 1–7, 1–8, and 1–9 deviated from the theoretical values dramatically. The largest deviation was the line velocity for 1–7, which represents the radial direction. Consequently, we can speculate that internal decay exists in the central area of the cross section, and the decay area is surrounded by the lines 1–5 and 1–9, which matches with the tomogram of sample 1–50 reasonably well as shown in Fig. 10.

6. Conclusions

With the assumption that the trunk of a tree under test is cylindrical and its cross section is in a round form, we developed a theoretical model of stress wave velocity in sound healthy trees and examined wave velocity patterns in the cross sections of 12 black cherry trees with experimental data. Our theoretical analysis indicated that the ratio of tangential velocity to radial velocity approximated a parabolic curve with symmetric axis $\theta = 0$ (θ is the angle between tangential direction and radial direction). The experimental results of 8 sound cross sections showed that the measured velocity patterns were in a good agreement with the theoretical analysis. The tomograms of 12 cross sections with internal decay reflected the anomaly of velocity pattern. The proposed theoretical velocity model can be used as a diagnostic tool to detect internal decay of live trees.

Acknowledgments

This research was made possible by the collaboration between the USDA Forest Service, Forest Products Laboratory and Zhejiang Agriculture and Forestry University in China. This study was supported in part by the Natural Science Foundation of China (Grant No. 61272313) and Zhejiang Provincial Science and Technology Project (Grant Nos. 2012C21015 and 2013C24026). The financial support to Dr. Guanghui Li's visiting study at the USDA Forest Productions Laboratory (FPL) was provided by the China Scholarship Council (CSC).

References

Bucur, V., 2003. Nondestructive Characterization and Imaging of Wood. Springer-Verlag, Berlin Heidelberg, Germany.

Dikrallah, A., Hakam, A., Kabouchi, B., Brancheriau, L., Bailleres, H., Famiri, A., Ziani, M., 2006. Experimental analysis of acoustic anisotropy of green wood by using guided waves. ESWM-COST Action E35, 149–154.

Divos, F., Divos, P., 2005. Resolution of stress wave based acoustic tomography. In: 14th International Symposium on Nondestructive Testing of Wood, pp. 309–314.

Gao, S., Wang, X., Wang, L., Allison, R.B., 2012. Effect of temperature on acoustic evaluation of standing trees and logs: Part 1—Laboratory investigation. Wood Fiber Sci. 44 (3), 286–297.

Kazemi, S., Shalbafan, A., Ebrahimi, G., 2009. Internal decay assessment in standing beech trees using ultrasonic velocity measurement. Eur. J. For. Res. 128 (4), 345–350.

Liang, S., Fu, F., Lin, L., Hu, N., 2010. Various factors and propagation trends of stress waves in cross sections of Euphrates poplar. For. Prod. J. 60 (5), 440–446.

Maurer, H.R., Schubert, S.I., Bachle, F., Clauss, S., Gsell, D., Dual, J., Niemz, P., 2005. Application of nonlinear acoustic tomography for nondestructive testing of trees. In: 14th International Symposium on Nondestructive Testing of Wood, pp. 339–349.

Pellerin, R.F., Ross, R.J., 2002. Nondestructive Evaluation of Wood. Forest Products Society, Madison, WI.

Wang, X., Wiedenbeck, J., Liang, S., 2009. Acoustic tomography for decay detection in black cherry trees. Wood Fiber Sci. 41 (2), 127–137.